1402 *Chem. Mater.* **2010,** *22,* 1402–1409
DOI:10.1021/cm9022024

CHEMISTRY OF MATERIALS
Article

Novel Stannite-type Complex Sulfide Photocatalysts A^I_2-Zn-A^{IV}-S_4 (A^I = Cu and Ag; A^{IV} = Sn and Ge) for Hydrogen Evolution under Visible-Light Irradiation

Issei Tsuji,[†] Yoshiki Shimodaira,[†] Hideki Kato,[†,§] Hisayoshi Kobayashi,[‡] and Akihiko Kudo*,[†]

[†]*Department of Applied Chemistry, Faculty of Science, Tokyo University of Science, 1-3 Kagurazaka, Shinjuku-Ku, Tokyo 162-0825, Japan and* [‡]*Department of Chemistry and Materials Technology, Kyoto Institute of Technology, Matsugasaki, Sakyo-ku, Kyoto 606-8585, Japan.* [§]*Present address: Institute of Multidisciplinary Research for Advanced Materials, Tohoku University, Japan.*

Received July 20, 2009. Revised Manuscript Received December 12, 2009

Photophysical properties and photocatalytic activities for H_2 evolution of the series of stannite-type complex sulfides A^I_2-Zn-A^{IV}-S_4 (A^I = Cu and Ag; A^{IV} = Sn and Ge) were studied. Diffuse reflection spectra and the plane-wave-based density functional theory (DFT) calculation suggested that the conduction bands were made up of Ge4s4p or Sn5s5p with S3p orbitals, while the valence bands consisted of Cu3d and Ag4d with S3p orbitals. The constituting elements of A^I and A^{IV} affected the photophysical and photocatalytic properties. Ru cocatalyst-loaded Cu_2ZnGeS_4, Ag_2ZnGeS_4, and Ag_2ZnSnS_4 showed high activities for photocatalytic H_2 evolution from an aqueous Na_2S+K_2SO_3 solution under visible-light irradiation. Combination of Cu and Ag made it possible that the $CuAgZnSnS_4$ photocatalyst with a narrow band gap (1.4 eV) utilized a wide range of visible light for the H_2 evolution.

1. Introduction

The development of a highly active photocatalyst for solar water splitting can lead to the realization of a green and sustainable energy system without fossil fuels. However, photogenerated electrons and holes in a tiny photocatalyst particle have to get over some harsh steps to reach the surface without their recombination and successfully carry out the water splitting on catalytic active sites.[1,2] New visible-light-driven photocatalysts for H_2 or O_2 evolution using sacrificial reagents and the useful new information for the development of photocatalyst materials have been reported. However, the number of such photocatalyst materials is not enough to establish the guiding principle for development of highly active photocatalysts for solar water splitting. It is important to develop a library of photocatalyst materials to see the factors affecting photocatalytic performances.

For the design of visible-light-driven photocatalysts, to focus attention on a band structure of materials is important at the first step. It is necessary that the conduction and valence band potentials satisfy the thermodynamic conditions for water splitting and the band gap is narrow enough to absorb visible light. Constituting elements and crystal structures of photocatalyst materials are important factors governing the above requirements. Inoue et al. have systematically developed a lot of ultraviolet-light-driven photocatalysts for overall water splitting in recognizing the importance of metal ions with d^{10} electronic configuration.[3] Present authors have reported new photocatalysts with valence bands which consist of some metal orbitals besides O2p orbitals. Mixed oxides, such as $AgNbO_3$,[4] Ag_3VO_4,[5] $SnNb_2O_6$,[6,7] and $BiVO_4$[8] having metal ions of Ag^+ with d^{10}, and Sn^{2+} and Bi^{3+} with $5s^2$ and $6s^2$ electronic configurations, showed photocatalytic activities for H_2 or O_2 evolution with sacrificial reagents under visible-light irradiation. Carrying out a band structure calculation for complex photocatalyst materials is now popular in this research field. Density functional theory (DFT) calculation of a band structure and measurement of photoelectrochemistry, photoelectron spectroscopy, and photophysical properties such as diffuse reflectance and photoluminescence spectra enable us to obtain detailed information about the energy band structure of photocatalyst materials and the relationship between the photocatalytic activity and the energy band structure.

Present authors have successfully developed unique visible-light-driven photocatalysts by applying the techniques

*Corresponding author phone: +81-35228-8267; fax: +81-35261-4631; e-mail: a-kudo@rs.kagu.tus.ac.jp.

(1) Osterloh, F. E. Chem. Mater., **2008**, *20*, 35, and references therein.
(2) Kudo, A.; Miseki, Y. Chem. Soc. Rev. **2009**, *38*, 253, and references therein.
(3) Inoue, Y. Energy Environ. Sci. **2009**, *2*, 364, and reference therein.
(4) Kato, H.; Kobayashi, H.; Kudo, A. *J. Phys. Chem. B* **2002**, *106*, 12441.
(5) Konta, R.; Kato, H.; Kobayashi, H.; Kudo, A. *Phys. Chem. Chem. Phys*. **2003**, *5*, 3061.
(6) Hosogi, Y.; Tanabe, K.; Kato, H.; Kobayashi, H.; Kudo, A. *Chem. Lett*. **2004**, *33*, 28.
(7) Hosogi, Y.; Shimodaira, Y.; K.; Kato, H.; Kobayashi, H.; Kudo, A. *Chem. Mater*. **2008**, *20*, 1299.
(8) Kudo, A.; Omori, K.; Kato, H. *J. Am. Chem. Soc*. **1999**, *121*, 11459.

 Published on Web 01/06/2010

of semiconductor band engineering to control of the band structures of photocatalyst materials. One example is the solid solution photocatalyst between ZnS with high activity for H_2 evolution under ultraviolet-light irradiation[9,10] and $MInS_2$ (M = Cu and Ag) with narrow band gaps. The series of solid solution photocatalysts show high activities for H_2 evolution even under simulated solar irradiation.[11−14] The band structure calculation in combination with the photophysical analyses for the solid solutions revealed that the visible-light-response was due to the contribution of Cu3d and Ag4d orbitals to the valence band and that of In5s5p orbitals to the conduction band. Zn4s4p orbitals that make up the conduction band in the solid solutions play an important role to maintain the conduction band energy level high enough to reduce H_2O to form H_2.

Stannite-type A^I_2-Zn-A^{IV}-S_4 (A^I = Cu and Ag, A^{IV} = Sn and Ge) compounds are quaternary complex sulfides whose crystal structures are similar to a zinc-blende structure of ZnS and a chalcopyrite structure of $CuInS_2$. Each metal cation is tetrahedrally coordinated by four sulfur anions. The structures of $Cu_2ZnA^{IV}S_4$ (A^{IV} = Sn and Ge) containing Cu as a monovalent ion have been investigated in detail. There are alternating cation layers of mixed Zn and A^{IV} atoms, which are separated from each other by layers of Cu atoms.[15,16] The stannite-type complex sulfides (selenides) have been studied as candidates for efficient low-cost solar cell materials,[17−23] especially as indium-free materials, and will attract attention as a new functional material in other fields. Present authors have aimed at the stannite-type complex sulfides as new visible-light-driven photocatalysts, because the constituting elements such as Cu, Ag, and Zn will contribute to the valence and conduction band formation as observed for ZnS-$CuInS_2$−$AgInS_2$ solid solution photocatalyst. The crystal structures of the stannite-type complex sulfides are similar to those of the visible-light-driven photocatalysts such as CdS,[24−26] Ni or Cu-doped ZnS,[27,28] and ZnS-$CuInS_2$−$AgInS_2$ solid solutions[11−14] with zinc-blende-type and wurtzite-type structures. Furthermore, sulfide photocatalysts consisting of Sn and Ge elements and stannite-type materials consisting of Ag[29] have hardly been investigated. Therefore, the study of the series of stannite-type complex sulfides will give useful information for understanding photocatalytic phenomena.

In the present paper, photocatalytic activities for H_2 evolution under visible-light irradiation and photophysical properties of quaternary, ternary, and binary chalcogenides, Cu_2ZnGeS_4, Cu_2GeS_3, and ZnS, which have similar crystal structures consisting of cations and anions filling tetrahedral sites, were studied. Then, the comparison in photophysical and photocatalytic properties among the series of stannite-type A^I_2-Zn-A^{IV}-S_4 (A^I = Cu and Ag, A^{IV} = Sn and Ge) complex sulfides was discussed. Absorption bands of previously reported ZnS-$CuInS_2$−$AgInS_2$ solid solution photocatalysts were red-shifted by combination of Cu with Ag, compared with those of ZnS-$CuInS_2$ and ZnS-$AgInS_2$ solid solution photocatalysts.[11−14] The extension of a wavelength range of available photon to a long wavelength and the improvement of photocatalytic performances for H_2 evolution were observed. Therefore, the effects of combination of Cu with Ag on the band structure and photocatalytic property were also examined for the stannite-type complex sulfides.

2. Experiment Section

Preparation of Photocatalysts. A precursor of Cu_2ZnSnS_4 was prepared by the following method. An aqueous solution (150 mL) of $Zn(NO_3)_2 \cdot 6H_2O$ (Wako Pure Chemicals; 99.0%) with 10−15% excess amounts (about 0.029 mol/L) and $SnCl_4 \cdot 5H_2O$ (Kanto Chemical; 98%) (0.025 mol/L) was purged with N_2 gas. CuCl was added into the mixture solution. This CuCl was freshly prepared by reduction of $CuCl_2$ (Wako Pure Chemicals; 99.0%) (about 0.07 mol) with metallic Cu plates (about 5 g) in a boiling diluted hydrochloric acid (about 4 mol/L, 150 mL) for 2−3 h. The fresh precipitate was washed with N_2-purged water and acetone. The obtained white precipitate of CuCl was dried in vacuo. A precursor of Cu_2ZnSnS_4 was precipitated with bubbling with an H_2S gas into the mixed solution containing $Zn(NO_3)_2$, $SnCl_4$, and CuCl. A precursor of Ag_2ZnSnS_4 was prepared as follows. A mixed aqueous solution (150 mL) of $Zn(NO_3)_2 \cdot 6H_2O$ with 10−15% excess amounts (about 0.029 mol/L) and $SnCl_4 \cdot 5H_2O$ (0.025 mol/L) was bubbled with an H_2S gas. Then, an aqueous solution containing of 7.5 mmol of $AgNO_3$ (Tanaka Kikinzoku; 99.8%) was slowly added into the mixed solution. The precursor of $CuAgZnSnS_4$ was also prepared by the same manner. These precursors of Cu_2ZnSnS_4, Ag_2ZnSnS_4, and $CuAgZnSnS_4$ were aged in H_2S-saturated water for about 5 h, washed with the H_2S-saturated water, and dried in air. The precursor of Cu_2ZnSnS_4 was pretreated at 573 K for 5 h under N_2 flow to eliminate sulfur formed by decomposition of a $Cu^{II}S$ impurity. The obtained dark brown powders of the precursors of Cu_2ZnSnS_4, Ag_2ZnSnS_4, and $CuAgZnSnS_4$ were heat-treated at 723−823 K for 10 h in evacuated quartz ampule tubes to prepare their crystallized materials.

Cu_2ZnGeS_4 and Ag_2ZnGeS_4 powders were synthesized by solid-state reactions. The starting materials, ZnS (99.999%),

(9) Reber, J. F.; Meier, K. *J. Phys. Chem. B* **1984**, *88*, 5903.
(10) Zeug, N.; Bucheler, J.; Kisch, H. *J. Am. Chem. Soc.* **1985**, *107*, 1459.
(11) Tsuji, I.; Kato, H.; Kobayashi, H.; Kudo, A. *J. Am. Chem. Soc.* **2004**, *126*, 13406.
(12) Tsuji, I.; Kato, H.; Kobayashi, H.; Kudo, A. *J. Phys. Chem. B* **2005**, *109*, 7323.
(13) Tsuji, I.; Kato, H.; Kudo, A. *Angew. Chem., Int. Ed.* **2005**, *44*, 3565.
(14) Tsuji, I.; Kato, H.; Kudo, A. *Chem. Mater.* **2006**, *18*, 1969.
(15) Schafer, W.; Nitsche, R. *Mater. Res. Bull.* **1974**, *9*, 645.
(16) Yao, G. Q.; Shen, H. S.; Honig, E. D.; Kershaw, R.; Dwight, K.; Wold, A. *Solid State Ionics* **1987**, *24*, 249.
(17) Matsushita, H.; Ochiai, T.; A, K. *J. Cryst. Growth* **2005**, *275*, 995.
(18) Katagiri, H. *Thin Solid Films* **2005**, *480−481*, 426.
(19) Doverspike, K.; Dwight, K.; Wold, A. *Chem. Mater.* **1990**, *2*, 194.
(20) Tanaka, K.; Miyamoto, Y.; Uchiki, H.; Nakazawa, K.; Araki, H. *Phys. Status Solidi A* **2006**, *203*, 2891.
(21) Scragg, J. J.; Dale, P. J.; Peter, L. M. *Electrochem. Commun.* **2008**, *10*, 639.
(22) Chen, S.; Gong, X. G.; Walsh, A.; Wei, S.-H. *Appl. Phys. Lett.* **2009**, *94*, 41903.
(23) Zhang, X.; Shi, X.; Ye, W.; Ma, C.; Wang, C. *Appl. Phys. A: Mater. Sci. Process.* **2009**, *94*, 381.
(24) Mau, A. W.-H.; Huang, C. B.; Kakuta, N.; Bard, A. J. *J. Am. Chem. Soc.* **1984**, *106*, 6537.
(25) Matsumura, M.; Furukawa, S.; Saho, Y.; Tsubomura, H. *J. Phys. Chem.* **1985**, *89*, 1327.
(26) Reber, J. F.; Rusek, M. *J. Phys. Chem.* **1986**, *90*, 824.
(27) Kudo, A.; Sekizawa, M. *Catal. Lett.* **1999**, *58*, 241.
(28) Kudo, A.; Sekizawa, M. *Chem. Commun.* **2000**, 1371.
(29) Johan, Z.; Picot, P. *Bull. Mineral.* **1982**, *105*, 229.

GeS_2 (99.99%), Cu_2S (99%), and Ag_2S (99%) purchased from Kojundo Chemical, were mixed with 15% excess amounts of zinc and germanium sulfides. The mixture was sealed in a quartz ampule tube in vacuo and heat-treated at 823−923 K for 10 h.

Characterization of Photocatalysts. The prepared materials were confirmed to be expected ones by X-ray diffraction (Rigaku; MiniFlex). Surface areas were determined by an N_2 BET method (Coulter; SA3100). Diffuse reflection spectra were obtained using a UV−vis−NIR spectrometer (Jasco; Ubest U-570) and were converted from reflection to absorbance by the Kubelka−Munk method. X-ray photoelectron spectra (XPS) were measured using an X-ray photoelectron spectrometer (VG Scientific; ESCALAB-MK). Binding energies were corrected by use of the Zn3d peak of ZnS at 10.5 eV.[30] Photocatalyst powders were observed by scanning electron microscopy (JEOL; JSM-7400F).

Photocatalytic Reactions. Photocatalytic reactions were conducted in a gastight circulation system. The photocatalyst powder (0.3 g) was dispersed by a magnetic stirrer in an aqueous solution (150 mL) containing K_2SO_3 and/or Na_2S as electron donors in a Pyrex cell with a top window. The photocatalysts were irradiated with visible light ($\lambda \geq 420$ nm) through a cutoff filter (Hoya L42) from a 300-W Xe lamp (Parkin-Elmer; Cermax-PE300BF). Cocatalysts of Ru, Rh, and Pt were photodeposited using appropriate amounts of $(NH_4)_2[RuCl_6]$ (Wako Chemicals; 29.9% as Ru), $RhCl_3 \bullet 3H_2O$ (Tanaka Kikinzoku; 39.45% as Rh), and $H_2PtCl_6 \bullet 6H_2O$ (Tanaka Kikinzoku; 37.5% as Pt) in the reactant solution containing K_2SO_3 and/or Na_2S in situ or in an aqueous K_2SO_3 solution in advance of the usage. The amount of H_2 evolved was determined with online gas chromatography (Shimadzu GC-8A, MS-5A column, TCD, Ar carrier). The apparent quantum yields defined by eq 1 were measured using filters combined with band-pass (Kenko) and cutoff (Hoya) filters and a photodiode (Ophir, PD300-UV head and Nova power monitor).

$$\text{A.Q.Y.}(\%) = \frac{\text{The number of reacted electrons}}{\text{The number of incident photons}} \times 100 = \frac{\text{The number of evolved } H_2 \text{ molecules} \times 2}{\text{The number of incident photons}} \times 100 \quad (1)$$

Band Structure Calculation. The band structure calculations of Cu_2ZnGeS_4 and Cu_2GeS_3 were carried out using the plane-wave-based density functional theory (DFT) program package Castep.[31] The valence atomic configurations of Cu_2ZnGeS_4 and Cu_2GeS_3 were $3d^{10}4s^1$, $3d^{10}4s^2$, $4s^24p^2$, and $3s^23p^4$ for Cu, Zn, Ge, and S atoms, respectively, with the ultrasoft core potentials.[32] The numbers of electrons in the primitive unit cell were 124 and 88 for $[Cu_2ZnGeS_4]_2$ and $[Cu_2GeS_3]_2$, respectively. The singlet states were assumed, and the numbers of occupied bands were the half of the numbers of electrons. The kinetic energy cutoff was set to 300 eV.

3. Results and Discussion

Characterization of Stannite-type Cu_2ZnGeS_4 Compared with ZnS and Cu_2GeS_3. Figure 1 shows X-ray diffraction patterns of ZnS, Cu_2ZnGeS_4, and Cu_2GeS_3. These sulfides have similar crystal structures with corner-shared tetrahedrons consisting of sulfur anions and metal cations. Zinc-blende-type ZnS with a cubic system has the highest symmetry in the sulfides.[33] Distorted Cu_2GeS_3 has a monoclinic system.[34] Stannite-type Cu_2ZnGeS_4, which is regarded as a solid solution between equimolar ZnS and Cu_2GeS_3, has a tetragonal system.[35] The Cu_2ZnGeS_4 synthesized at 923 K was the low-temperature phase of stannite-type. A wurtzite-type high-temperature phase was not confirmed. The XRD peaks of Cu_2GeS_3 and Cu_2ZnGeS_4 were partially split because of their distorted symmetries being different from those of ZnS with a high symmetry. The diffraction peaks of the sulfides shifted to higher angles as the ratio of Ge was increased. The successive shift is reasonable because the ion radius of Ge^{4+} (0.53 Å) is smaller than those of Zn^{2+} (0.74 Å) and Cu^+ (0.74 Å).[36] The excess Zn and Ge were added in the starting materials as mentioned in the Experimental Section. The addition would suppress isolation of impurities such as Ag_2S and Cu_2S or formation of Cu^{2+} accompanied with forming vacancies of Ag^+ and Cu^+ sites due to the charge compensation.

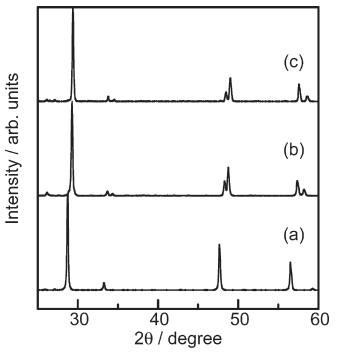

Figure 1. X-ray diffraction patterns of (a) ZnS prepared at 923 K, (b) Cu_2ZnGeS_4 prepared at 923 K, and (c) Cu_2GeS_3 prepared at 1073 K.

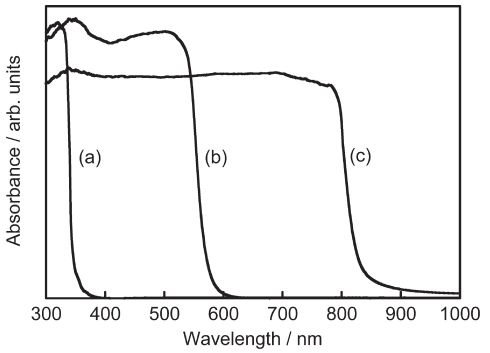

Figure 2. Diffuse reflection spectra of (a) ZnS prepared at 923 K, (b) Cu_2ZnGeS_4 prepared at 923 K, and (c) Cu_2GeS_3 prepared at 1073 K.

Figure 2 shows the diffuse reflection spectra of the ZnS, Cu_2ZnGeS_4, and Cu_2GeS_3. The wide band gap

(30) Xu, J. F.; Ji, W.; Lin, J. Y.; Tang, S. H.; Du, Y. W. *Appl. Phys. A: Mater. Sci. Process.* **1998**, *66*, 639.
(31) Payne, M. C.; Teter, M. P.; Allan, D. C.; Arias, T. A.; Joannopoulos, J. D. *Rev. Mod. Phys.* **1992**, *64*, 1045.
(32) Vanderbilt, D. *Phys. Rev.* **1990**, *B41*, 7892.
(33) Yeh, C.; Lu, Z. W.; Froyen, S.; Zunger, A. *Phys. Rev. B* **1992**, *46*, 10086.
(34) de Chalbaud, L. M.; Diaz de Delgado, G.; Delgado, J. M.; Mora, A. E.; Sagredo, V. *Mater. Res. Bull.* **1997**, *32*, 1371.
(35) Ottenburgs, G. *Bull. Soc. Fr. Mineral. Cristallogr.* **1972**, *95*, 458.
(36) Shannon, R. *Acta Crystallogr., Sect. A: Found. Crystallogr.* **1976**, *32*, 751.

semiconductor ZnS absorbed only ultraviolet light (BG: 3.6 eV). On the other hand, Cu_2GeS_3 with a narrow band gap (BG: 1.5 eV) possessed a wide absorption band in a visible-light region up to around 830 nm. An absorption edge of Cu_2ZnGeS_4 (BG: 2.2 eV) was in position between those of ZnS and Cu_2GeS_3. The relationship between the compositions and the absorption bands suggested that Cu and Ge orbitals contributed to the energy band formation for visible-light absorption.

DFT calculation was carried out in order to obtain the detailed information about the band structure of Cu_2ZnGeS_4 and Cu_2GeS_3. Figure 3(a) shows the partial density of states for Cu, Zn, Ge, and S atoms of Cu_2ZnGeS_4. The contribution of S3p orbitals appeared in both valence and conduction bands due to the partial covalent bond formation. The Cu3d orbitals showed a strong contribution near the valence band maximum and raised the valence band potential to a high-energy side. Figure 3(b) shows the electron density contour maps for the highest occupied molecular orbital (HOMO) and the lowest unoccupied molecular orbital (LUMO). The HOMO was made up of Cu3d and S3p hybrid orbitals, and the LUMO consisted of Ge4s4p and S3p hybrid orbitals. The large contribution of the Ge4s4p and S3p orbitals to the conduction band was also observed from the partial density of states (Figure 3(a)). The amplitude of Zn4s4p orbitals appeared at a little higher-energy side than the LUMO. The conduction band potential would be maintained at comparatively high level by the contribution of the Zn4s4p orbitals. Inoue et al. carried out DFT calculation of the band structure for a Zn_2GeO_4 photocatalyst.[37] That result showed that the conduction band (LUMO) was formed with Ge4s4p orbitals with small contribution of the Zn4s4p orbitals. The calculation result of Zn_2GeO_4 was similar to that of Cu_2ZnGeS_4 for the conduction band. The valence and conduction bands of Cu_2GeS_3 mainly consisted of Cu3d+S3p and Ge4s4p+S3p hybrid orbitals, respectively, as shown in Figure 3 (c) and (d). The bottom of the conduction band of Cu_2ZnGeS_4 was higher than that of Cu_2GeS_3, judging from energy levels of Ge4s in their partial DOSs.

Photocatalytic Property of Stannite-type Cu_2ZnGeS_4 Compared with ZnS and Cu_2GeS_3. Table 1 shows the photocatalytic activities of ZnS, Cu_2ZnGeS_4, and Cu_2GeS_3 for H_2 evolution from an aqueous solution containing S^{2-} and SO_3^{2-} as sacrificial reagents under visible-light irradiation ($\lambda \geq 420$ nm). The stannite-type Cu_2ZnGeS_4 showed a slight activity for H_2 evolution without a cocatalyst. The photocatalytic activity was drastically increased when a Ru cocatalyst of an active site for H_2 evolution was loaded on the Cu_2ZnGeS_4 powder. This result indicated that the conduction band level of the Cu_2ZnGeS_4 photocatalyst was thermodynamically suitable for the H_2 evolution. However, the driving force that is the potential difference between the conduction band level and a reduction potential of H_2O to form H_2 was not kinetically enough. The Ru cocatalyst that works as H_2 evolution site kinetically assisted the

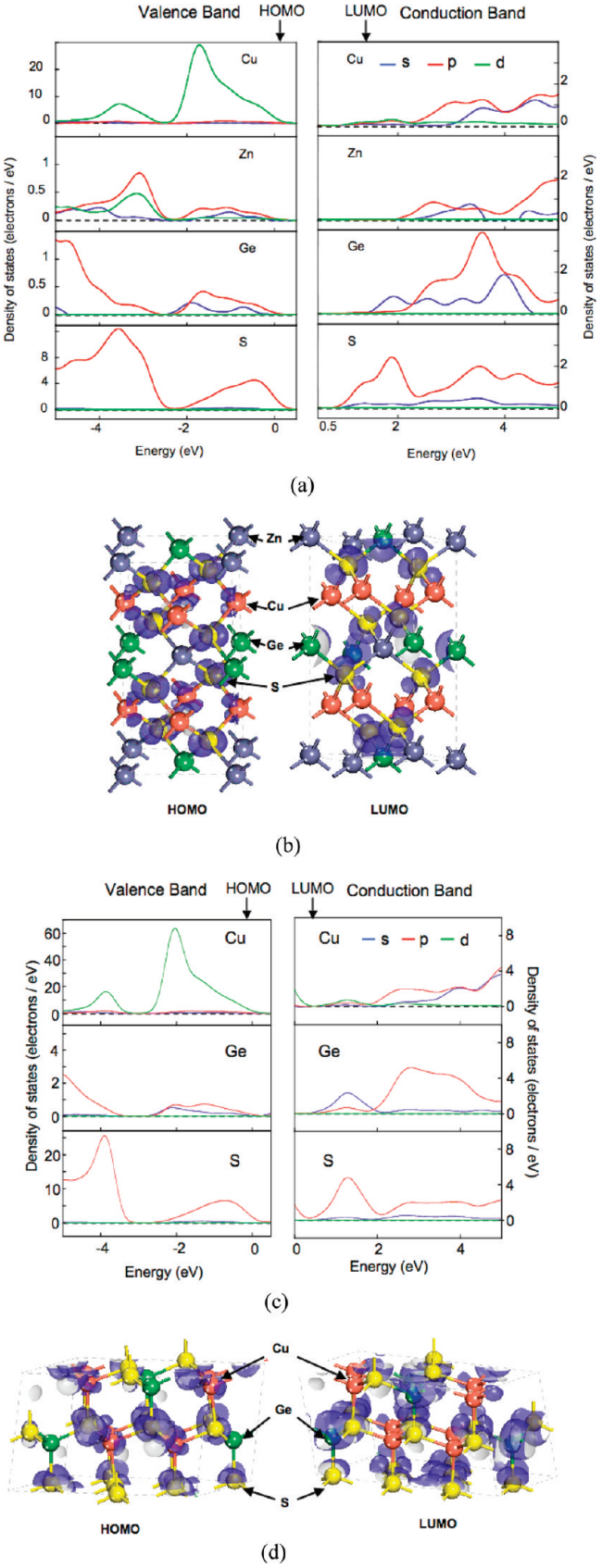

Figure 3. (a) Partial density of state (DOS) for Cu, Zn, Ge, and S atoms and (b) electron density contour maps for HOMO and LUMO of Cu_2ZnGeS_4. (c) Partial density of state (DOS) for Cu, Ge, and S atoms and (d) electron density contour maps for HOMO and LUMO of Cu_2GeS_3.

(37) Sato, J.; Kobayashi, H.; Ikarashi, K.; Saito, N.; Nishiyama, H.; Inoue, Y. *J. Phys. Chem. B* **2004**, *108*, 4369.

Table 1. Photocatalytic Activities for H_2 Evolution from an Aqueous K_2SO_3 and Na_2S Solution over ZnS, Cu_2ZnGeS_4, and Cu_2GeS_3 under Visible-Light Irradiation[c]

photocatalysts	preparation temperature/K	cocatalysts	BET surface area/$m^2\ g^{-1}$	band gap/eV	rate of H_2 evolution/μmol h^{-1}
Cu_2ZnGeS_4	923	none	1.4	2.2	4.5
Cu_2ZnGeS_4	923	Pt[a]	1.4	2.2	13
Cu_2ZnGeS_4	923	Rh[a]	1.4	2.2	50
Cu_2ZnGeS_4	923	Ru[a]	1.4	2.2	324
Cu_2ZnGeS_4	923	Ru[b]	1.4	2.2	294
ZnS	923	Ru[b]	1.5	3.6	1.4
Cu_2GeS_3	1073	Ru[b]	0.5	1.5	0.1

[a] Cocatalysts (0.5 wt %) were photodeposited in an aqueous K_2SO_3 solution in advance of the usage. [b] Cocatalysts (0.5 wt %) were photodeposited in the reactant solution in situ. [c] Catalyst: 0.3 g, Reactant solutions: 0.5 mol L^{-1} K_2SO_3 + 0.1 mol L^{-1} Na_2S solution 150 mL, Light source: 300 W Xe lamp ($\lambda \geq 420$ nm).

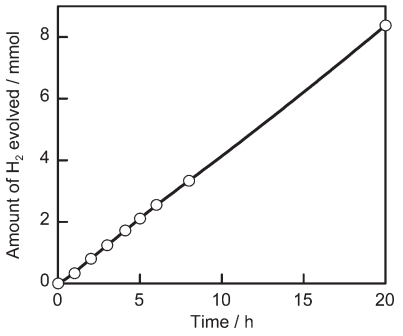

Figure 4. Photocatalytic H_2 evolution from an aqueous 0.35 M Na_2S + 0.25 M K_2SO_3 solution under visible-light irradiation over a Ru (0.5 wt %)-loaded Cu_2ZnGeS_4. Catalyst: 0.3 g, light source: 300 W Xe lamp with a cutoff filter ($\lambda \geq 420$ nm), reaction cell: top window Pyrex cell.

reduction of H_2O to form H_2. A conventional Pt cocatalyst for H_2 evolution was not effective in this system. ZnS with a high conduction band showed high activity without cocatalyst under UV irradiation,[9,10] but little activity under visible-light irradiation because of its wide band gap (3.6 eV). Cu_2GeS_3 did not produce H_2 even though it absorbed a wide range of visible light. Cu_2GeS_3 did not seem to have the conduction band potential high enough to reduce H_2O to form H_2, unlike Cu_2ZnGeS_4. DFT calculations for Cu_2GeS_3 and Cu_2ZnGeS_4 suggested that the conduction band potential of Cu_2ZnGeS_4 was higher than that of Cu_2GeS_3 because Zn4s4p orbitals drew up the bottom of the conduction band of Cu_2ZnGeS_4. However, the conduction band level of Cu_2ZnGeS_4 located at lower energy side than that of ZnS, due to the strong contribution of Ge4s4p orbitals around the LUMO, resulting in that the Cu_2ZnGeS_4 photocatalyst required a cocatalyst such as Ru to produce H_2 efficiently, in contrast to the ZnS photocatalyst.

Figure 4 shows the amount of H_2 produced over the Ru(0.5 wt %)-loaded Cu_2ZnGeS_4 photocatalyst in an aqueous K_2SO_3 (0.25 mol L^{-1}) and Na_2S (0.35 mol L^{-1}) solution under visible-light irradiation ($\lambda \geq 420$ nm). The activity of the photocatalyst was comparatively stable over 20 h of a reaction time. The initial rate of H_2 evolution was 455 μmol h^{-1}. The photocatalyst showed the low activity (26 μmol h^{-1}) from an aqueous Na_2S (0.35 mol L^{-1}) solution and hardly possessed the activity from aqueous K_2SO_3 (0.25 mol L^{-1}) solution. The high activity was obtained only from the aqueous solution containing both S^{2-} and SO_3^{2-} ions. In this reactant solution, the photocatalytic reaction is supposed to proceed along the following processes[9]

$$\text{Photocatalyst} + h\nu \rightarrow e^-(\text{CB}) + h^+(\text{VB}) \quad (2)$$

$$2H_2O + 2e^-(\text{CB}) \rightarrow H_2 + 2OH^- \quad (3)$$

$$SO_3^{2-} + H_2O + 2h^+(\text{VB}) \rightarrow SO_4^{2-} + 2H^+ \quad (4)$$

$$2S^{2-} + 2h^+(\text{VB}) \rightarrow S_2^{2-} \quad (5)$$

$$S_2^{2-} + SO_3^{2-} \rightarrow S_2O_3^{2-} + S^{2-} \quad (6)$$

$$SO_3^{2-} + S^{2-} + 2h^+(\text{VB}) \rightarrow S_2O_3^{2-} \quad (7)$$

H_2O is reduced to H_2 by the electrons photogenerated in the conduction band accompanied by oxidation of sacrificial reagents. The photogenerated holes in the valence band oxidize SO_3^{2-} and S^{2-} to form SO_4^{2-} and S_2^{2-} directly, according to eqs 4 and 5, respectively. The production of S_2^{2-} ions, which act as an optical filter and compete with the reduction of protons, was efficiently suppressed by mixing with SO_3^{2-} ions, according to eqs 6 and 7. The presence of excess S^{2-} ions in the reaction solution also stabilizes the photocatalyst surface because the formation of sulfur defects could be suppressed.

Characterization of A^I_2-Zn-A^{IV}-S_4 (A^I = Cu and Ag, A^{IV} = Sn and Ge). Figure 5 shows X-ray diffraction patterns of A^I_2-Zn-A^{IV}-S_4 (A^I = Cu and Ag, A^{IV} = Sn and Ge). We have previously reported the ZnS-$CuInS_2$−$AgInS_2$ solid solution photocatalyst for H_2 evolution.[13,14] Combination of Cu with Ag elements caused the extension of a wavelength range of available photon to a long wavelength, improving the photocatalytic performance for H_2 evolution on the ZnS-$CuInS_2$−$AgInS_2$ solid solution photocatalyst, compared with ZnS-$CuInS_2$ and ZnS-$AgInS_2$ solid solution photocatalysts. In this expectation of the same effect for the stannite-type sulfide photocatalysts, the $CuAgZnSnS_4$ complex sulfide that was a combined system between Cu_2ZnSnS_4 and Ag_2ZnSnS_4 was also synthesized. The diffraction patterns of synthesized Cu_2ZnGeS_4 and Cu_2ZnSnS_4 containing

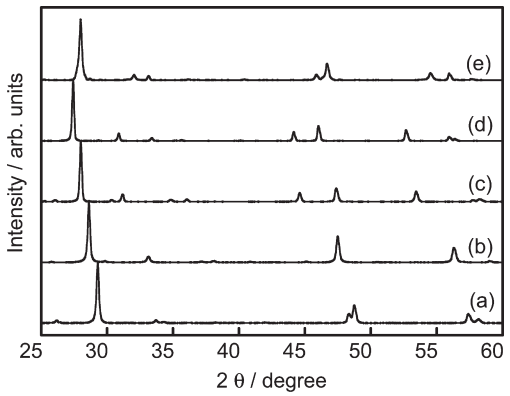

Figure 5. X-ray diffraction patterns of (a) Cu_2ZnGeS_4 prepared at 923 K, (b) Cu_2ZnSnS_4 prepared at 823 K, (c) Ag_2ZnGeS_4 prepared at 823 K, (d) Ag_2ZnSnS_4 prepared at 723 K, and (e) $CuAgZnSnS_4$ prepared at 823 K.

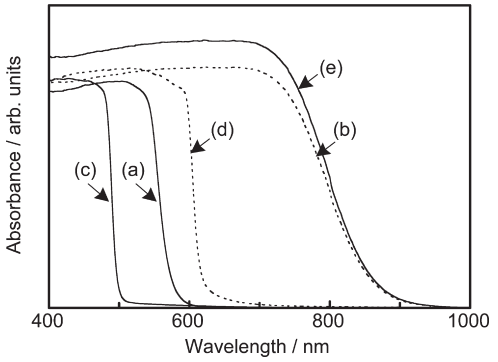

Figure 6. Diffuse reflection spectra of (a) Cu_2ZnGeS_4 prepared at 923 K, (b) Cu_2ZnSnS_4 prepared at 823 K, (c) Ag_2ZnGeS_4 prepared at 823 K, (d) Ag_2ZnSnS_4 prepared at 723 K, and (e) $CuAgZnSnS_4$ prepared at 823 K.

monovalent Cu agreed well with those reported by Schafer[15] and Ottenburgs,[35] respectively. On the other hand, it has been reported by Johan that the crystal phase of Ag_2ZnSnS_4 with monovalent Ag was identified to be a stannite-like structure.[29] The Ag_2ZnGeS_4 complex sulfide has never been reported as far as the authors know. The diffraction pattern of Ag_2ZnGeS_4 was similar to that of Ag_2ZnSnS_4 and was regarded as the stannite-like structure. The XRD patterns of Ag_2ZnGeS_4 and Ag_2ZnSnS_4 containing monovalent Ag shifted to lower angles compared with those of Cu_2ZnGeS_4 and Cu_2ZnSnS_4 containing monovalent Cu, because the ionic radius of Ag^+ (1.14 Å) was larger than that of Cu^+ (0.74 Å).[36] The XRD pattern of $CuAgZnSnS_4$ was also according to this manner. The splits of XRD peaks of Ag_2ZnGeS_4 and Ag_2ZnSnS_4 indicated that the symmetries of the crystal structures were broken due to the presence of Ag^+ ions with a large size.

Figure 6 shows the diffuse reflection spectra of $A^I{}_2$-Zn-A^{IV}-S_4 (A^I = Cu and Ag, A^{IV} = Sn and Ge). Cu_2ZnGeS_4 and Cu_2ZnSnS_4 containing monovalent Cu had absorption bands at longer wavelengths than Ag_2ZnGeS_4 and Ag_2ZnSnS_4 containing monovalent Ag because Cu3d orbitals formed higher valence bands than Ag4d orbitals. The same relationship between the absorption bands and monovalent ions has been observed for ZnS-$CuInS_2$ and ZnS-$AgInS_2$ solid solutions.[11,12] DFT calculations of

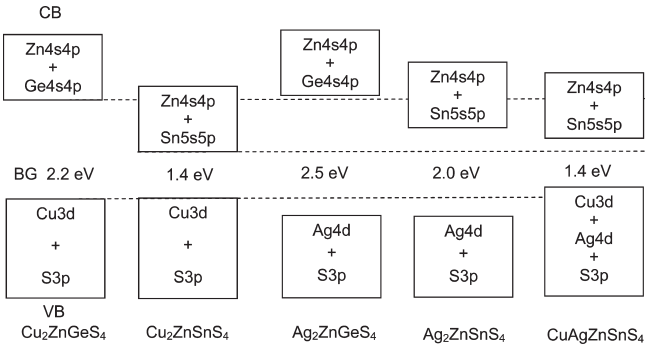

Figure 7. Relative band levels of $A^I{}_2$-Zn-A^{IV}-S_4 (A^I = Cu and Ag, A^{IV} = Sn and Ge).

these sulfide solid solutions revealed that the valence band composed of the Cu3d and S3p hybrid orbitals was formed at a more negative level than that of Ag4d and S3p hybrid orbitals.[11−14] The valence band characters of $A^I{}_2$-Zn-A^{IV}-S_4 (A^I = Cu and Ag, A^{IV} = Sn and Ge) should be similar to those of ZnS-$CuInS_2$ and ZnS-$AgInS_2$ solid solutions. Cu_2ZnSnS_4 and Ag_2ZnSnS_4 containing Sn had the absorption bands at longer wavelengths than the Cu_2ZnGeS_4 and Ag_2ZnGeS_4 consisting of Ge. The conduction band minima consisted of Ge4s4p orbitals as indicated by DFT calculation of Cu_2ZnGeS_4 (Figure 3). It has been reported that Sn^{4+} of the same group cation as Ge^{4+} with d^{10} electronic configuration contributes to the conduction band formation.[22] The band gaps of Cu_2ZnSnS_4 and Ag_2ZnSnS_4 were narrower than those of Cu_2ZnGeS_4 and Ag_2ZnGeS_4, suggesting that Sn5s5p orbitals contributed to the conduction band formations at lower energy sides than Ge4s4p orbitals. On the other hand, Ag_2ZnSnS_4 had a larger crystal-structural distortion than Cu_2ZnSnS_4, judging from the splits of XRD patterns. This distortion resulted in the raise of the conduction band of Ag_2ZnSnS_4 compared with Cu_2ZnSnS_4, even if their conduction band minima consisted of Sn5s5p orbitals. The above discussion based on diffuse reflection spectra and DFT calculations including the previous reports give a band structure of $A^I{}_2$-Zn-A^{IV}-S_4 as shown in Figure 7.

It is noteworthy that the band gap of $CuAgZnSnS_4$ was the same as that of Cu_2ZnSnS_4. In general, it would been expected that the absorption edge of $CuAgZnSnS_4$, which was regarded as the solid solution between equimolar Cu_2ZnSnS_4 and Ag_2ZnSnS_4, would be in a position between those of Cu_2ZnSnS_4 and Ag_2ZnSnS_4 as observed for the ZnS-Ge_2SnS_3 solid solution as shown in Figure 2. However, for the stannite-type complex sulfides, the absorption edge of $CuAgZnSnS_4$ was located at the same position as that of Cu_2ZnSnS_4 (ca. 860 nm). This behavior is similar to that of the ZnS-$CuInS_2$−$AgInS_2$ solid solution photocatalyst.[13,14] This band gap narrowing by the combination of Cu with Ag can be explained as follows. The crystal structure of $CuAgZnSnS_4$ was distorted more largely than that of Cu_2ZnSnS_4 because of substituted Ag atoms with a large size. Therefore, the crystal field around Cu cations was changed by the substitution of the Ag cations. The energy state of Cu orbitals would be affected

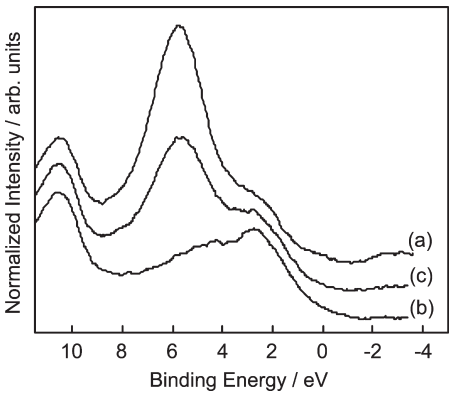

Figure 8. X-ray photoelectron spectra of (a) Ag_2ZnSnS_4, (b) Cu_2ZnSnS_4, and (c) $CuAgZnSnS_4$.

by this change, resulting in widening the valence band and raising the top. At the same time, the conduction band minimum of $CuAgZnSnS_4$ was slightly high compared with that of Cu_2ZnSnS_4, because of the crystal structural distortion of $CuAgZnSnS_4$ as shown in Figure 7. That is one of the possible reasons why the band gap of $CuAgZnSnS_4$ was almost the same as that of Cu_2ZnSnS_4. Figure 8 shows X-ray photoelectron spectra of valence bands for Cu_2ZnSnS_4, Ag_2ZnSnS_4, and $CuAgZnSnS_4$. All peaks observed at 10.5 eV were assigned to Zn3d. Ag_2ZnSnS_4 showed a distinctive peak around 5.7 eV derived from Ag4d and a small shoulder at a low energy side. The Cu_2ZnSnS_4 showed a small peak around 2.8 eV hidden in an entirely broad peak, which would be derived from Cu3d orbitals. On the other hand, $CuAgZnSnS_4$ combined with Cu and Ag showed a similar peak around 5.7 eV to Ag_2ZnSnS_4. In addition to that, the peak around 2.8 eV, which looked like a larger shoulder than that of Ag_2ZnSnS_4, was observed for $CuAgZnSnS_4$ as well as Cu_2ZnSnS_4. Therefore, it was revealed that the both of the Cu3d and Ag4d orbitals contributed to the valence band formation of the $CuAgZnSnS_4$. Taking the results of XPS into consideration, another possible reason why the band gap of $CuAgZnSnS_4$ was almost the same as that of Cu_2ZnSnS_4 can be considered. That is the interaction among the Zn3d, Cu3d, and Ag4d energy bands that repels the valence band maximum upward, resulting in the widening of the valence band and the absorption band of the $CuAgZnSnS_4$ as observed for the ZnS-$CuInS_2$–$AgInS_2$ solid solution photocatalysts.

Photocatalytic Property of A^I_2-Zn-A^{IV}-S_4 (A^I = Cu and Ag, A^{IV} = Sn and Ge). Table 2 shows the photocatalytic activities of A^I_2-Zn-A^{IV}-S_4 (A^I = Cu and Ag, A^{IV} = Sn and Ge) for H_2 evolution from an aqueous solution containing S^{2-} and SO_3^{2-} as sacrificial reagents under visible-light irradiation ($\lambda \geq 420$ nm). Figure 9 shows time courses of H_2 evolution under visible-light irradiation over Ru-loaded Ag_2ZnSnS_4, Cu_2ZnSnS_4, and $CuAgZnSnS_4$. Ag_2ZnGeS_4 and Ag_2ZnSnS_4 complex sulfides were active photocatalysts for H_2 evolution, in addition to the Cu_2ZnGeS_4 photocatalyst as shown in Table 1 and Figure 4. Cu_2ZnSnS_4 hardly possessed the photocatalytic activity even with a similar chemical

Table 2. Photocatalytic Activities for H_2 Evolution from an Aqueous K_2SO_3 and Na_2S Solution over Stannite-type A^I_2-Zn-A^{IV}-S_4 (A^I = Cu and Ag; A^{IV} = Sn and Ge) under Visible-Light Irradiation

photocatalysts[a]	preparation temperature/K	BET surface area/m^2 g^{-1}	band gap/eV	rate of H_2 evolution/ μmol h^{-1}
Cu_2ZnGeS_4	923	1.4	2.2	323
Cu_2ZnSnS_4	823	5.9	1.4	2
Ag_2ZnGeS_4	823	0.6	2.5	370
Ag_2ZnSnS_4	723	0.8	2.0	482
$CuAgZnSnS_4$	823	0.5	1.4	304

[a] Ru cocatalyst: 0.5 wt % loaded. Catalyst: 0.3 g, reactant solutions: 0.5 mol L^{-1} K_2SO_3 + 0.1 mol L^{-1} Na_2S solution 150 mL, light source: 300 W Xe lamp ($\lambda \geq 420$ nm).

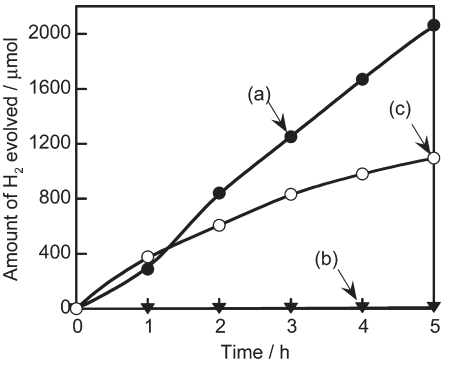

Figure 9. Photocatalytic H_2 evolution from an aqueous 0.35 M Na_2S + 0.25 M K_2SO_3 solution under visible-light irradiation over Ru (0.5 wt %)-loaded (a) Ag_2ZnSnS_4, (b) Cu_2ZnSnS_4, and (c) $CuAgZnSnS_4$. Catalyst: 0.3 g, light source: 300 W Xe lamp with a cutoff filter ($\lambda \geq 420$ nm), reaction cell: top window Pyrex cell.

composition to the active Cu_2ZnGeS_4 photocatalyst because the conduction band consisting of Sn5s5p orbitals would possess poor potential to reduce H_2O to form H_2. In contrast to it, Ag_2ZnSnS_4 of which the conduction band consisted of Sn5s5p orbitals showed a high photocatalytic activity for H_2 evolution. The Ag_2ZnSnS_4 photocatalyst with the high potential of the conduction band and the narrow band gap of 2.0 eV showed the highest activity among the stannite-type sulfides tested in the present study as shown Table 2.

The $CuAgZnSnS_4$ photocatalyst with a narrow band gap (1.4 eV) showed a comparatively high activity (304 μmol h^{-1}) for H_2 evolution, although the activity was not as high as the Ag_2ZnSnS_4 photocatalyst. However, it was interesting that the high activity was obtained by the combination of Cu with Ag, whereas Cu_2ZnSnS_4 with the same band gap as $CuAgZnSnS_4$ hardly possessed the photocatalytic activity for H_2 evolution. This might be due to the fact that the crystal structure of $CuAgZnSnS_4$ was slightly distorted, resulting in that the conduction band located at an enough high energy level to produce H_2 as well as the Ag_2ZnSnS_4 photocatalyst as shown in Figure 7.

The Cu_2ZnGeS_4 produced H_2 gas most stably in the stannite-type complex sulfides as shown in Figure 4, whereas the Ag_2ZnGeS_4, Ag_2ZnSnS_4, and $CuAgZnSnS_4$ photocatalysts containing monovalent Ag showed some deactivation during the photocatalytic reaction as shown in Figure 9. A part of Ag^+ cations near the surface might

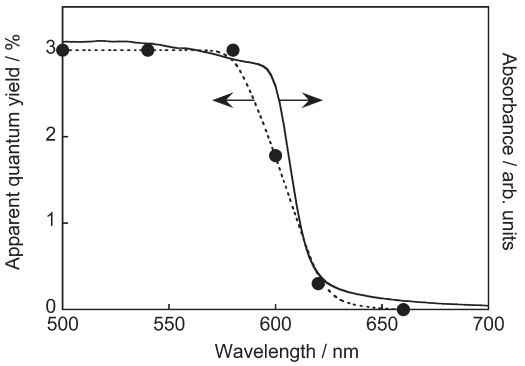

Figure 10. An action spectrum of H_2 evolution from an aqueous 0.1 M Na_2S + 0.5 M K_2SO_3 solution over Ru (0.5 wt %)-loaded Ag_2ZnSnS_4 photocatalyst. Catalyst: 0.3 g, light source: 300 W Xe lamp with cutoff and band-pass filters, reaction cell: top window Pyrex cell.

be reduced to form metallic Ag by photogenerated electrons for the Ag-containing photocatalysts, resulting in the deactivation.

Figure 10 shows an action spectrum for H_2 evolution from an aqueous solution containing SO_3^{2-} and S^{2-} ions over Ru(0.5 wt %)-loaded Ag_2ZnSnS_4 photocatalyst that showed the highest activity among the stannite-type sulfide photocatalysts tested in the present study. The onset of the action spectrum agreed well with the onset of the diffuse reflection spectrum. It indicated that the visible-light response was due to the band gap transition. The wide range of visible light up to 620 nm was available to produce H_2 over the Ru-loaded Ag_2ZnSnS_4 photocatalyst.

Figure 11 shows electron microscope images of the Cu_2ZnGeS_4 and Ag_2ZnSnS_4 photocatalysts which showed the high photocatalytic activities. The SEM measurement revealed that the particle sizes of Cu_2ZnGeS_4 and Ag_2ZnSnS_4 were a few hundred nanometers and several micrometers, respectively. The well-crystallized particles were observed. Ag_2ZnSnS_4 showed higher photocatalytic activity for H_2 evolution than Cu_2ZnGeS_4, even if the particle size was larger and the surface area was smaller than those of Cu_2ZnGeS_4. This result indicated that the high activity of Ag_2ZnSnS_4 was not due to such properties. It can be expected that controlling the particle size by refining a preparation method makes it possible to improve the photocatalytic activity.

Conclusions

Stannite-type A^I_2-Zn-A^{IV}-S_4 (A^I = Cu, Ag; A^{IV} = Sn, Ge) compounds have arisen as the new series of photocatalysts for H_2 evolution from an aqueous solution containing S^{2-} and SO_3^{2-} under visible-light irradiation ($\lambda \geq 420$ nm). It was found that stannite-type compounds consisting of Ag and/or Ge were especially unique photofunctional materials. Ag_2ZnSnS_4 was the most active photocatalyst among them. Cu_2ZnGeS_4 also showed a high activity, and the stability was superior to that of Ag_2ZnSnS_4. The crystal systems and the band structures changed with the size and frontier orbitals of cations, A^I and A^{IV}. Crystal structural distortion by existing of monovalent Ag with a large size also affected the band position, resulting in improvement of photocatalytic

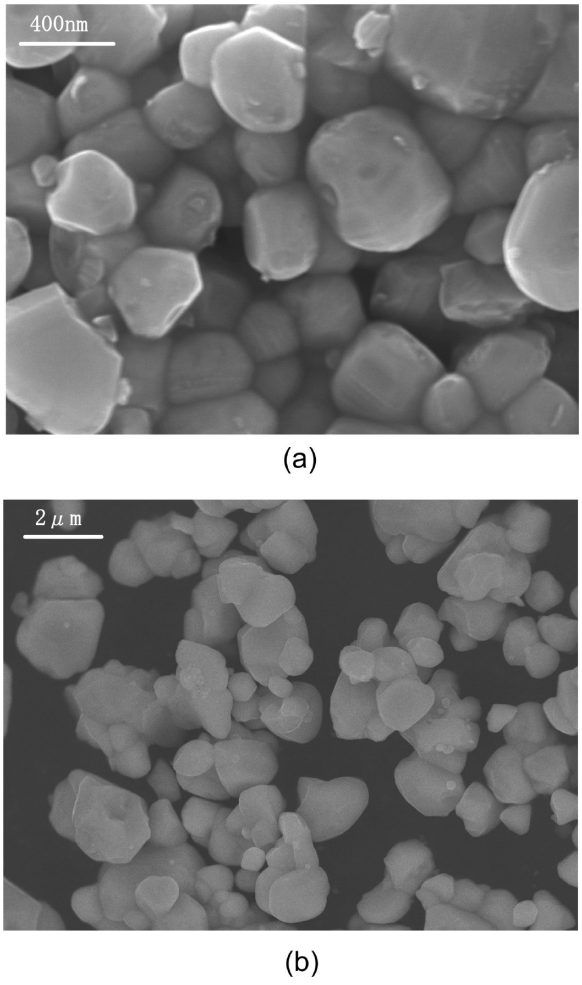

Figure 11. Scanning electron microscope images of (a) Cu_2ZnGeS_4 prepared at 923 K and (b) Ag_2ZnSnS_4 prepared at 723 K.

activity. The visible-light response of the photocatalysts was associated with the contribution of Cu3d and Ag4d orbitals to the valence band and Ge4s4p and Sn5s5p orbitals to the conduction band. $CuAgZnSnS_4$ with a narrow band gap (1.4 eV) showed a photocatalytic activity for H_2 evolution, whereas the photocatalytic activity of Cu_2ZnSnS_4 with the same band gap was negligible. This result indicates the synergetic effect of coexistence of monovalent Cu and Ag. These findings are expected to give useful information on the strategy for development of new photocatalyst materials. This photocatalytic H_2 evolution using metal sulfide photocatalysts will be important if abundant sulfur compounds in chemical industries or nature can be used as electron donors, even though it is not a solar energy conversion reaction. Ideally, this reaction produces H_2 at ambient temperature and pressure but does not consume fossil fuels and does not emit CO_2. Moreover, these materials can be used for photoelectrode systems and solar cells.[38]

Acknowledgment. This work was supported by a Grant-in-Aid for Priority Area Researches from the Ministry of Education, Culture, Science, and Technology of Japan.

(38) Guo, Q.; Hillhouse, H. W.; Agrawal, R. *J. Am. Chem. Soc.* **2009**, *131*, 11672.